Liquid-gas phase transition in strange hadronic matter with relativistic models

James R. Torres,[1,*] F. Gulminelli,[2,†] and Débora P. Menezes[1,‡]
[1]*Departamento de Física, CFM, Universidade Federal de Santa Catarina, Florianópolis, C.P. 476, CEP 88040-900, Santa Catarina, Brazil*
[2]*CNRS and ENSICAEN, UMR6534, LPC, 14050 Caen Cédex, France*
(Received 27 October 2015; published 3 February 2016)

Background: The advent of new dedicated experimental programs on hyperon physics is rapidly boosting the field, and the possibility of synthesizing multiple strange hypernuclei requires the addition of the strangeness degree of freedom to the models dedicated to nuclear structure and nuclear matter studies at low energy.
Purpose: We want to settle the influence of strangeness on the nuclear liquid-gas phase transition. Because of the large uncertainties concerning the hyperon sector, we do not aim at a quantitative estimation of the phase diagram but rather at a qualitative description of the phenomenology, as model independent as possible.
Method: We analyze the phase diagram of low-density matter composed of neutrons, protons, and Λ hyperons using a relativistic mean field (RMF) model. We largely explore the parameter space to pin down generic features of the phase transition, and compare the results to *ab initio* quantum Monte Carlo calculations.
Results: We show that the liquid-gas phase transition is only slightly quenched by the addition of hyperons. Strangeness is seen to be an order parameter of the phase transition, meaning that dilute strange matter is expected to be unstable with respect to the formation of hyperclusters.
Conclusions: More quantitative results within the RMF model need improved functionals at low density, possibly fitted to *ab initio* calculations of nuclear and Λ matter.

DOI: 10.1103/PhysRevC.93.024306

I. INTRODUCTION

It is well known that nuclear matter below saturation exhibits a first-order phase transition belonging to the liquid-gas (LG) universality class [1–9]. The study of the associated phase diagram is not only a playground for many-body theorists, but it is also of clear relevance for nuclear phenomenology, since the very existence of atomic nuclei can be understood as a finite-size manifestation of that phase transition. In a similar way, one can ask whether the existence of hypernuclei as bound systems implies the presence of a similar phase transition in the extended phase diagram where strangeness represents an extra dimension.

Since the first synthesis of Λ hypernuclei in the 1980s, numerous nuclear matter studies including hyperons have been performed [10–15]. These early studies assumed very attractive couplings in the strange sector in order to justify the extra binding measurements of double-Λ hypernuclei [16,17]. As a consequence, it was predicted that multistrange clusters and even strangelets could be stable and possibly accessible in heavy-ion collisions. In particular, in Ref. [14] the occurrence of a thermodynamic phase transition in strange compressed baryonic matter was predicted, which would lead to a new family of neutron stars characterized by much smaller radii than usually considered.

However, more recent analyses [18,19] of double-Λ hypernuclei tend to suggest a very small attraction in the Λ-Λ channel, and the stability of pure Λ matter seems to be ruled out. Most hypernuclear matter studies are nowadays essentially motivated by assessing the strange content of neutron star cores, and therefore concentrate on matter in β equilibrium [20]. At β equilibrium, no hyperons appear below baryonic densities of the order of $3\rho_0$ or more. For this reason, the influence of strangeness on the low-density nuclear matter phase diagram has never been studied, to our knowledge. Still, the existence of single- and double-Λ hypernuclei, and the very active research on multiply strange nuclei with the advent of new dedicated experimental programs such as J-Parc in Japan or PANDA at FAIR (Facility for Antiproton and Ion Research, Darmstadt) [21–24] suggests that the nuclear liquid-gas phase transition should be preserved by the consideration of the strangeness degree of freedom [25].

In this paper, we explore the influence of strangeness on the LG phase transition with popular relativistic mean-field (RMF) models. Like in any other phenomenological effective model, the couplings of the RMF are not fully known even at subsaturation densities. In particular, neutron star physics has taught us in the recent years that it is important to go beyond a simple SU(6) or even SU(3) symmetry, and extra attractive σ^* and repulsive ϕ mesons specifically coupled to the strange baryons should be introduced [26–31], which leads to a potentially uncontrolled multiplication of parameters. However, if we limit ourselves to the simple system composed of neutrons, protons, and Λ hyperons, nuclear and hypernuclear structures provide some constraints that can be used to limit the parameter space of the model. In this paper, we consider the simple linear and nonlinear Walecka model for the $np\Lambda$ system, and discuss the modification of the nuclear matter phase diagram under a wide variation of coupling constants, in the acceptable parameter space constrained both from hypernuclear data and *ab initio* calculations of hypernuclear matter. We show that in the whole parameter space the LG phase transition is preserved by the addition of strangeness, even if the extension of the spinodal along the strange density direction is subject to large uncertainties. The instability zone is globally quenched by

*james.r.torres@posgrad.ufsc.br
†gulminelli@lpccaen.in2p3.fr
‡debora.p.m@ufsc.br

strangeness, but the strange density is an order parameter of the transition. This means that, from the thermodynamic point of view, the formation of hyperclusters with multiple Λ's should be favored at low density [22–24], which has possible implications in relativistic heavy-ion collisions [25].

The paper is organized as follows. Section II briefly recalls the main equations of the Walecka model, in both its linear and nonlinear versions, for the $npΛ$ system with inclusion of strange mesons. Section III defines the coupling parameter space of the model, under the constraints of well defined values for the Λ potential as required by the available hypernuclear data. To further refine the domain of acceptable parameters, Sec. IV compares the RMF functionals with recent *ab initio* predictions of $n\Lambda$ matter with the auxiliary field diffusion Monte Carlo (AFDMC) technique [32]. In Sec. V the general formalism for the analysis of spinodal instabilities in multicomponent systems is revisited. The main results of our work are presented in Sec. VI, which shows in detail the instability properties of $n\Lambda$ and $npΛ$ matter with the different choices for the couplings. Finally, Sec. VII summarizes the paper.

II. FORMALISM

In this section, we present the hadronic equation of state (EOS) used in this work. We describe matter within the framework of relativistic mean field (RMF) models involving the interaction of Dirac baryons mediated by the scalar and vector mesons which are independent degrees of freedom [33–40]. The scalar-isoscalar σ field mediates the medium-range attraction between baryons, the vector-isoscalar ω field mediates the short-range repulsion between baryons, the strange scalar σ^* field mediates the medium-range attraction between hyperons, the strange vector ϕ field mediates the short-range repulsion between hyperons, and finally the ρ meson field allows us to adjust isovector properties of nuclear matter. In the present work, we used the nonlinear Walecka model (NLWM) and the linear Walecka model (LWM), which can be obtained by just turning off the nonlinear terms, in the presence of the mesons listed above. Nonlinear means that there are also self-interaction terms for the scalar field σ in the Lagrangian density, as proposed by Boguta and Bodmer [34,41], which provides better results than the LWM [39]. The Lagrangian density reads

$$\mathcal{L} = \sum_j \overline{\psi}_j [\gamma^\mu (i\partial_\mu - g_{\omega j}\omega_\mu - g_{\phi j}\phi_\mu - g_{\rho j}\vec{\tau}\cdot\vec{\rho}_\mu) - m_j^*]\psi_j + \frac{1}{2}\left(\partial_\mu\sigma\,\partial^\mu\sigma - m_\sigma^2\sigma^2\right) - \frac{1}{3}bM_N(g_{\sigma N}\sigma)^3 - \frac{1}{4}c(g_{\sigma N}\sigma)^4$$
$$+ \frac{1}{2}\left(\partial_\mu\sigma^*\partial^\mu\sigma^* - m_\sigma^2\sigma^{*2}\right) - \frac{1}{4}\Omega_{\mu\nu}\,\Omega^{\mu\nu} + \frac{1}{2}m_\omega^2\,\omega_\mu\omega^\mu - \frac{1}{4}\Phi_{\mu\nu}\Phi^{\mu\nu} + \frac{1}{2}m_\phi^2\phi^\mu\phi_\mu, - \frac{1}{4}\vec{R}_{\mu\nu}\cdot\vec{R}^{\mu\nu} + \frac{1}{2}m_\rho^2\vec{\rho}_\mu\cdot\vec{\rho}^{\,\mu}, \quad (2.1)$$

where $m_j^* = m_j - g_{\sigma j}\,\sigma - g_{\sigma^* j}\,\sigma^*$ is the baryon effective mass and m_j is the bare mass of the baryon j. The terms $\Omega_{\mu\nu} = \partial_\mu\omega_\nu - \partial_\nu\omega_\mu$, $\Phi_{\mu\nu} = \partial_\mu\phi_\nu - \partial_\nu\phi_\mu$, and $\vec{R}_{\mu\nu} = \partial_\mu\vec{\rho}_\nu - \partial_\nu\vec{\rho}_\mu - g_{\rho j}(\vec{\rho}_\mu \times \vec{\rho}_\nu)$ are the strength tensors, where the up arrow in the last term denotes the isospin vectorial space with the $\vec{\tau}$ isospin operator. The coupling constants are $g_{ij} = \chi_{ij}g_{iN}$, with the mesons denoted by index $i = \sigma,\omega,\rho,\sigma^*,\phi$ and the baryons denoted by j. Note that χ_{ij} is a proportionality factor between g_{ij} and the nucleon coupling constants g_{iN}, with $N = n,p$. The couplings b and c are the weights of the nonlinear scalar terms. The sum over j can be extended over all baryons of the octet $(n,p,\Lambda,\Sigma^-,\Sigma^0,\Sigma^+,\Xi^-,\Xi^0)$.

The values of the coupling constants of the nucleons with mesons σ, ω, and ρ are obtained from the phenomenology. These constants are tuned to the bulk properties of nuclear matter. Some of these properties are not known exactly, just within certain ranges, like the effective masses of the nucleons, therefore there are many sets of parameters that describe the bulk properties. The biggest uncertainties concern the hyperon coupling constants, because the phenomenological information from hypernuclei is not sufficient to completely pin down the interaction in the strange sector [42,43]. The hyperon couplings are chosen in different ways in the literature, either based on simple symmetry considerations [29,44–48] or requiring an EOS in β equilibrium sufficiently stiff to justify the observation of very massive neutron stars [49,50].

Some different approaches, all affected by a certain degree of arbitrariness, are listed here. (1) Some authors argue that $\chi_{\sigma j} = \chi_{\omega j} = \chi_{\rho j} = \sqrt{2/3}$ [45]. (2) In another work [46], the authors claim that $\chi_{\sigma\Lambda} = \chi_{\omega\Lambda} = \chi_{\sigma\Sigma} = \chi_{\omega\Sigma} = 2/3$, $\chi_{\sigma\Xi} = \chi_{\omega\Xi} = 1/3$, $\chi_{\rho\Lambda} = 0$, $\chi_{\rho\Sigma} = 2$ and $\chi_{\rho\Xi} = 0$. (3) Based on the experimental analysis of Λ-hypernuclei data, an alternative constraint is given by $U_\Lambda(n_N = n_0) = \chi_{\omega\Lambda}(g_{\omega N}) - \chi_{\sigma\Lambda}(g_{\sigma N}) = -28$ MeV for the fixed $\chi_{\sigma\Lambda} = 0.75$. This last case can be extended to the whole baryonic octet, indexed by j, setting $\chi_{\sigma j} = 0.75$; $\chi_{\omega j}$ is given by the above constraint and $\chi_{\rho h} = 0$, where h is the hyperon index [49]. (4) Another approach is to take into account the resulting neutron star maximum mass [49,50].

In the case of the inclusion of the strange mesons, σ^* and ϕ [26–28], we have to ensure that the nuclear matter properties are preserved when these new mesons are included. New mesons mean new interactions and also new constants, therefore the arbitrariness introduced by these constants must be eliminated by data whenever possible. In analogy with what has been done with the $g_{\sigma\Lambda}$, when constrained by the hypernuclear potential U_Λ^N via hypernuclear data [49], we can try to tie the strange constants to the U_Λ^Λ data available in literature [18,19,47,51–58]. In the next section we develop these ideas in detail.

Applying the Euler-Lagrange equations to the Lagrangian density Eq. (2.1) and using the mean-field approximation [37] $(\sigma \to \langle\sigma\rangle = \sigma_0;\ \omega_\mu \to \langle\omega_\mu\rangle = \delta_{\mu 0}\,\omega_0;\ \vec{\rho}_\mu \to \langle\vec{\rho}_\mu\rangle =$

$\delta_{\mu 0}\,\delta^{i3}\rho_0^3 \equiv \delta_{\mu 0}\,\delta^{i3}\rho_{03}$; $\sigma^* \to \langle\sigma^*\rangle = \sigma_0^*$; $\phi_\mu \to \langle\phi_\mu\rangle = \delta_{\mu 0}\,\phi_0$), we obtain the following equations of motion for the meson fields at zero temperature:

$$
\begin{aligned}
(g_{\sigma N}\sigma_0) &= \Delta_\sigma\left(\sum_j \chi_{\sigma j}\rho_j^s - bM_n(g_{\sigma N}\sigma_0)^2 - c(g_{\sigma N}\sigma_0)^3\right),\\
(g_{\omega N}\omega_0) &= \Delta_\omega\sum_j \chi_{\omega j} n_j,\\
(g_{\rho N}\rho_0) &= \Delta_\rho\sum_j \tau_{3j}\chi_{\rho j} n_j,\\
(g_{\sigma N}\sigma_0^*) &= \Delta_{\sigma\sigma^*}\sum_j \chi_{\sigma^* j}\rho_j^s,\\
(g_{\omega N}\phi_0) &= \Delta_{\omega\phi}\sum_j \chi_{\phi j} n_j,
\end{aligned}
\tag{2.2}
$$

where for simplicity we define the following factors: $\Delta_\sigma = (\frac{g_{\sigma N}}{m_\sigma})^2$, $\Delta_\omega = (\frac{g_{\omega N}}{m_\omega})^2$, $\Delta_\rho = (\frac{g_{\rho N}}{m_\rho})^2$, $\Delta_{\sigma\sigma^*} = (\frac{g_{\sigma N}}{m_{\sigma^*}})^2$, $\Delta_{\omega\phi} = (\frac{g_{\omega N}}{m_\phi})^2$; $\chi_{\sigma j}$, $\chi_{\sigma^* j}$, $\chi_{\omega j}$, $\chi_{\rho j}$, and $\chi_{\phi j}$ are ratios between coupling constants and τ_{3j} is the third component of the isospin projection of the j baryon. The scalar and baryon densities are given respectively by

$$\rho_j^s = \frac{\gamma}{2\pi^2}\int_0^{k_{Fj}} \frac{m_j^*}{\sqrt{p^2+m_j^{*2}}}p^2dp \tag{2.3}$$

and

$$n_j = \frac{\gamma}{2\pi^2}\int_0^{k_{Fj}} p^2dp. \tag{2.4}$$

The energy density of the baryons is given by

$$\varepsilon_B = \frac{\gamma}{2\pi^2}\sum_j\int_0^{k_{Fj}} p^2\sqrt{p^2+m_j^{*2}}dp, \tag{2.5}$$

and for the mesons

$$
\begin{aligned}
\varepsilon_M = &\frac{(g_{\sigma N}\sigma_0)^2}{2\Delta_\sigma} + \frac{(g_{\omega N}\omega_0)^2}{2\Delta_\omega} + \frac{(g_{\rho N}\rho_0)^2}{2\Delta_\rho} + \frac{(g_{\sigma N}\sigma_0^*)^2}{2\Delta_{\sigma\sigma^*}}\\
&+ \frac{(g_{\omega N}\phi_0)^2}{2\Delta_{\omega\phi}} + \frac{1}{3}bM_n(g_{\sigma N}\sigma_0)^3 + \frac{1}{4}c(g_{\sigma N}\sigma_0)^4.
\end{aligned}
\tag{2.6}
$$

Finally the total energy density is the summation

$$\varepsilon = \varepsilon_B + \varepsilon_M.$$

To obtain the chemical potential, one has to take the derivatives of the energy density with respect to the baryon density [39]. Note the dependence of the Fermi momenta and the fields with the baryon density in the upper limit of the integrals in Eqs. (2.5) and (2.6) respectively. Using the derivative chain rule and the equation of motion for the σ field, we obtain

$$\mu_j^* = \mu_j - \chi_{\sigma j}(g_{\omega N}\omega_0) - \tau_{3j}\chi_{\rho j}(g_{\rho N}\rho_0) - \chi_{\omega j}(g_{\phi N}\phi_0). \tag{2.7}$$

The total pressure is

$$p = p_B + p_M,$$

where p_B is the baryonic pressure given by

$$p_B = \frac{\gamma}{2\pi^2}\sum_j\int_0^{k_{Fj}} \frac{p^4}{\sqrt{p^2+m_j^{*2}}}dp, \tag{2.8}$$

and p_M is the pressure of the mesons:

$$
\begin{aligned}
p_M = &-\frac{(g_{\sigma N}\sigma_0)^2}{2\Delta_\sigma} + \frac{(g_{\omega N}\omega_0)^2}{2\Delta_\omega} + \frac{(g_{\rho N}\rho_0)^2}{2\Delta_\rho} - \frac{(g_{\sigma N}\sigma_0^*)^2}{2\Delta_{\sigma\sigma^*}}\\
&+ \frac{(g_{\omega N}\phi_0)^2}{2\Delta_{\omega\phi}} - \frac{1}{3}bM_n(g_{\sigma N}\sigma_0)^3 - \frac{1}{4}c(g_{\sigma N}\sigma_0)^4.
\end{aligned}
\tag{2.9}
$$

III. LAMBDAS IN (HYPER)NUCLEAR MATTER

Inspired by the pioneer works on the role of the isospin in the liquid-gas phase transition [3,5,7,59–63], along with more recent works on the role of the strangeness in the phase transition of dense neutron-star matter [64–67], in this work we want to study the role of strangeness in the low-density and zero-temperature LG phase transition, which can be phenomenologically associated with multiple strange bound hypernuclei [24,25].

Because of the huge uncertainties in the strange sector we do not aim at having quantitative predictions on that phase transition, but would like to get qualitative statements and avoid as much as possible the model dependence of the results. For this reason we shall explore as widely as possible the largely unconstrained parameter space of the hyperon couplings. In this section we detail the criteria employed to fix the size of the parameter space.

Concerning the nucleon sector, we used the GM1 parametrization for the NLWM [45] and the original Walecka [37] parametrization for the LWM. The two sets of parameters, denoted by NLWM and LWM respectively, are shown in Table I with the fitted nuclear bulk properties.

It is well known that the value of the symmetric nuclear matter incompressibility does not qualitatively influence the phase diagram, nor do the uncertainties on the other parameters. We therefore consider the NLWM couplings as sufficiently well settled and do not play with them in the following. To fully

TABLE I. Sets of parameters used in this work and corresponding saturation properties.

	NLWM	LWM
n_0 (fm^{-3})	0.153	0.17
K (MeV)	300	554
m^*/m	0.70	0.54
B/A (MeV)	−16.3	−15.95
$\mathcal{E}_{\rm sym}$ (MeV)	32.5	39.22
L (MeV)	94	127.22
Δ_σ (fm^2)	11.785	13.670
Δ_ω (fm^2)	7.148	10.250
Δ_ρ (fm^2)	4.410	4.410
$\Delta_{\sigma\sigma^*}$ (fm^2)	3.216	3.769
$\Delta_{\omega\phi}$ (fm^2)	4.212	6.040
b	0.002947	0.000
c	−0.001070	0.000

explore the phenomenology of the model in the strange sector, the hyperon couplings are considered as free parameters, which, however, have to fulfill minimal requirements in terms of the potential and the hypernuclei data. To be clear with the notation in the following, the general function associated with the Λ potential is the three-variable function $\mathcal{U}_\Lambda(n_n,n_p,n_\Lambda)$. For symmetric matter $n_n = n_p$ we have a two-variable function $U_\Lambda(n_N,n_\Lambda)$. The one-variable ΛN potential is denoted by $U_\Lambda^N(n_N) \equiv U_\Lambda(n_N,n_\Lambda = 0)$, and finally for the $\Lambda\Lambda$ potential we have $U_\Lambda^\Lambda(n_\Lambda) \equiv U_\Lambda(n_N = 0,n_\Lambda)$, where $n_N = n_n + n_p$ is the nucleon density. For simplicity sometimes we omit the dependence of the potential function with respect to the density variables. The χ_Λ couplings tell us how attractive or repulsive the U_Λ can be. For the hyperon coupling constants, it is difficult to fix these phenomenological parameters due to the scarcity of data available, especially for the multihyperon nuclei. Hence when the σ^* and ϕ are taken into consideration we need some data from single-Λ and double-Λ nuclei. Based on data on single Λ produced in (π^+,K^+) reactions, the presently accepted value of the single Λ in symmetric nuclear matter at saturation density $U_\Lambda^N(n_0)$ is ≈ -28 MeV [54,55]. For multiple hyperons there are available data just for the double-Λ light nuclei, such as ${}^{10}_{\Lambda\Lambda}$Be, ${}^{13}_{\Lambda\Lambda}$Be, and ${}^{6}_{\Lambda\Lambda}$He, and the measurements are related to the $\Lambda\Lambda$ bond energy. This energy can be estimated from the binding energy difference between double-Λ and single-Λ hypernuclei denoted by $\Delta B_{\Lambda\Lambda}$. In this work we consider the value $\Delta B_{\Lambda\Lambda} = 0.67$ MeV [18,19,56–58]. The $\Delta B_{\Lambda\Lambda}$ can be interpreted as a rough estimation of the U_Λ^Λ potential at the average Λ density $\langle n_\Lambda\rangle \sim n_0/5$ inside the hypernucleus [55], where n_0 is the saturation point of symmetric nuclear matter in Table I. Hence, the $U_\Lambda^N(n_0) = -28$ MeV potential data can be used to tie the $\chi_{\omega\Lambda}$ to the $\chi_{\sigma\Lambda}$. For strange mesons, using $U_\Lambda^\Lambda(n_0/5) = -0.647$ MeV we intend to link the $\chi_{\phi\Lambda}$ to the $\chi_{\sigma^*\Lambda}$. The general form of the Λ potential U_Λ in the RMF models considered is given by

$$U_\Lambda(n_N,n_\Lambda) = \chi_{\omega\Lambda}(g_{\omega N}\omega_0) + \chi_{\phi\Lambda}(g_{\omega N}\phi_0) - \chi_{\sigma\Lambda}(g_{\sigma N}\sigma_0) - \chi_{\sigma^*\Lambda}(g_{\sigma N}\sigma_0^*), \tag{3.1}$$

where the dependence on the densities is given by the equations of motion of the meson fields, and n_N is the symmetric nuclear matter density. Nucleons and Λ's exchange σ and ω mesons with each other, the first one being attractive while the second acts repulsively. These two mesons have no strange quantum number. The additional strange mesons are similar to the ordinary σ and ω but they see just the strange baryons, namely hyperons. The attractive force is due to the scalar meson σ^* and the repulsive is due to the strange vector meson ϕ. For simplicity we can define $\omega = (g_{\omega N}\omega_0)$, $\phi = (g_{\omega N}\phi_0)$, $\sigma = (g_{\sigma N}\sigma_0)$, and $\sigma^* = (g_{\sigma N}\sigma_0^*)$ to rewrite Eq. (3.1) in terms of the densities instead of the fields:

$$U_\Lambda(n_N,n_\Lambda) = \chi_{\omega\Lambda}\left(\frac{g_{\omega n}}{m_\omega}\right)^2 n_N - \chi_{\sigma\Lambda}\left(\frac{g_{\sigma n}}{m_\sigma}\right)^2 \rho_N^s(\sigma) + \left[1 + \left(\frac{\chi_{\phi\Lambda}}{\chi_{\omega\Lambda}}\right)^2\left(\frac{m_\omega}{m_\phi}\right)^2\right]\left(\frac{g_{\omega n}}{m_\omega}\right)^2(\chi_{\omega\Lambda})^2 n_\Lambda - \left[1 + \left(\frac{\chi_{\sigma^*\Lambda}}{\chi_{\sigma\Lambda}}\right)^2\left(\frac{m_\sigma}{m_{\sigma^*}}\right)^2\right]\left(\frac{g_{\sigma n}}{m_\sigma}\right)^2(\chi_{\sigma\Lambda})^2\rho_\Lambda^s(\sigma,\sigma^*) - \chi_{\sigma\Lambda}\left(\frac{g_{\sigma n}}{m_\sigma}\right)^2[-bm_n\sigma^2 - c\sigma^3]. \tag{3.2}$$

We can look for one-dimensional potential $U_\Lambda^N(n_N)$, which is just the Λ potential for a Λ in nuclear symmetric matter, and this potential is a single-variable function in nucleon density. It reads

$$U_\Lambda^N(n_N) = \chi_{\omega\Lambda}\left(\frac{g_{\omega N}}{m_\omega}\right)^2 n_N - \chi_{\sigma\Lambda}\left(\frac{g_{\sigma N}}{m_\sigma}\right)^2 \times\left[\rho_N^s(\sigma) - bm_n\sigma^2 - c\sigma^3\right]. \tag{3.3}$$

Here we can use the data for $U_\Lambda^N(n_0) = -28$ MeV. Solving the above expression for $\chi_{\omega\Lambda}$ and using the equation of motion of the fields we have

$$\chi_{\omega\Lambda} = \frac{\chi_{\sigma\Lambda}\sigma|_{N=n_0} - 28\ \text{MeV}}{\omega|_{N=n_0}}. \tag{3.4}$$

The $\chi_{\sigma\Lambda}$ is left to be a free parameter in the RMF models. Figure 1 shows the relation between $\chi_{\sigma\Lambda}$ and $\chi_{\omega\Lambda}$ when we consider Eq. (3.4). For each choice of the $\chi_{\sigma\Lambda}$, a particular potential is obtained in such a way that it is constrained to $U_\Lambda^N(n_0;\chi_{\sigma\Lambda}) = -28$ MeV. The linear dependence obtained means that in the framework of the (N)LWM a strong attraction at low densities is always correlated to a strong repulsion at high densities. It is interesting to remark that the same is true in non-relativistic models [64–66].

Figure 2 shows the family of potentials constrained by Eq. (3.4) in LWM and NLWM. We can see that a very wide variety of behaviors is compatible with the hypernuclei constraint, which explains why dedicated RMF works to hypernuclear structure have been able in the literature to reasonably fit the available single-particle levels with a large variety of choices for the couplings. We can also observe that the LWM and NLWM models produce very similar behaviors for this potential. The main difference between the two models, for large $\chi_{\sigma\Lambda}$, is that the U_Λ^N potential in NLWM is deeper at low densities than the LWM due to the nonlinear terms and the parametrization chosen.

Now, we turn our attention to the $U_\Lambda^\Lambda(n_\Lambda)$ potential:

$$U_\Lambda^\Lambda(n_\Lambda) = \left[1 + \left(\frac{\chi_{\phi\Lambda}}{\chi_{\omega\Lambda}}\right)^2\left(\frac{m_\omega}{m_\phi}\right)^2\right](\chi_{\omega\Lambda})\omega - \alpha(\chi_{\sigma\Lambda})\Sigma, \tag{3.5}$$

where we have defined $\alpha = 1 + (\frac{\chi_{\sigma^*\Lambda}}{\chi_{\sigma\Lambda}})^2(\frac{m_\sigma}{m_{\sigma^*}})^2$ and

$$\Sigma = \sigma - \left(\frac{g_{\sigma N}}{m_\sigma}\right)^2\left(\frac{\alpha - 1}{\alpha}\right)(-bm_n\sigma^2 - c\sigma^3). \tag{3.6}$$

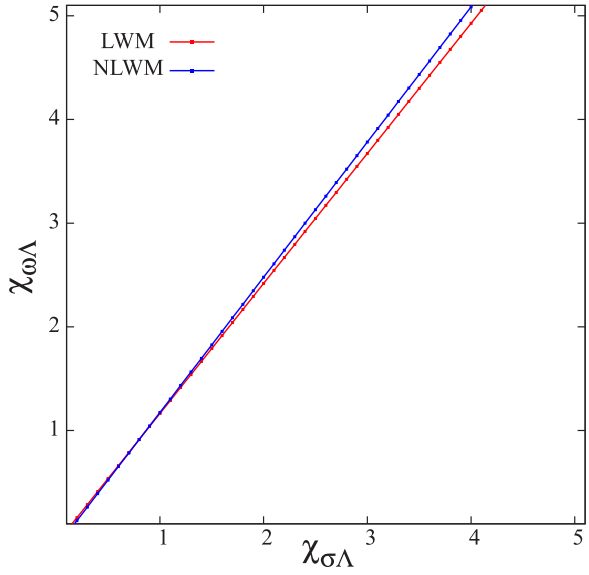

FIG. 1. Relations between parameters in RMF.

The other chosen data is $U_\Lambda^\Lambda(\frac{n_0}{5}) = -0.67$ MeV. Therefore, solving Eq. (3.5) for $\chi_{\phi\Lambda}$, we obtain

$$\chi_{\phi\Lambda} = \left(\frac{m_\phi}{m_\omega}\right) \times \sqrt{\frac{U_\Lambda^\Lambda\left(\frac{n_0}{5}\right) + \alpha\chi_{\sigma\Lambda}\Sigma|_{n_\Lambda=\frac{n_0}{5}} - \chi_{\omega\Lambda}\omega|_{n_\Lambda=\frac{n_0}{5}}}{\chi_{\omega\Lambda}\omega|_{n_\Lambda=\frac{n_0}{5}}}}\,\chi_{\omega\Lambda}. \tag{3.7}$$

The above expressions are valid for the NLWM, and the LWM expression is obtained for $b = c = 0$, when the Σ is reduced to the σ field. Figure 3 shows the three-dimensional (3D) parameter space $\chi_{\sigma\Lambda} \times \chi_{\sigma^*\Lambda} \times \chi_{\phi\Lambda}$ where we consider Eq. (3.7). Note that in Eq. (3.7) there are combinations of $\chi_{\sigma\Lambda}$ and $\chi_{\sigma^*\Lambda}$ that do not result in real solutions. This gives a first trivial limitation for the parameter values. The residual parameter space, shown in Fig. 3 for the NLWM, is still extremely large. Minimal constraints can be added requiring that convergent solutions are obtained in hyperonic stellar matter (with all the baryon octet, electrons, and muons included) in β equilibrium. $\chi_\rho = 1.5$ is fixed, so that we guarantee that Λ's are the first hyperons to appear and the (unconstrained) couplings to Σ do not play a major role. The gray points in Fig. 3 are related to divergent solutions, where the Λ effective mass goes to zero at some finite density. The red points yield possible solutions and, in some cases, the maximum masses can reach two solar masses with a finite Y_Λ [29,30].

This study is only done with the NLWM because it is well known that the LWM leads to unrealistic results for high-density matter. Of course the LWM and NLWM give different EOS even at low density, but for now it is enough to restrict our parameter space substantially to start the study of possible instabilities in hypernuclear matter at low density. Later, we see how drastic our choice for the $\chi_{\sigma\Lambda}$ parameter is when

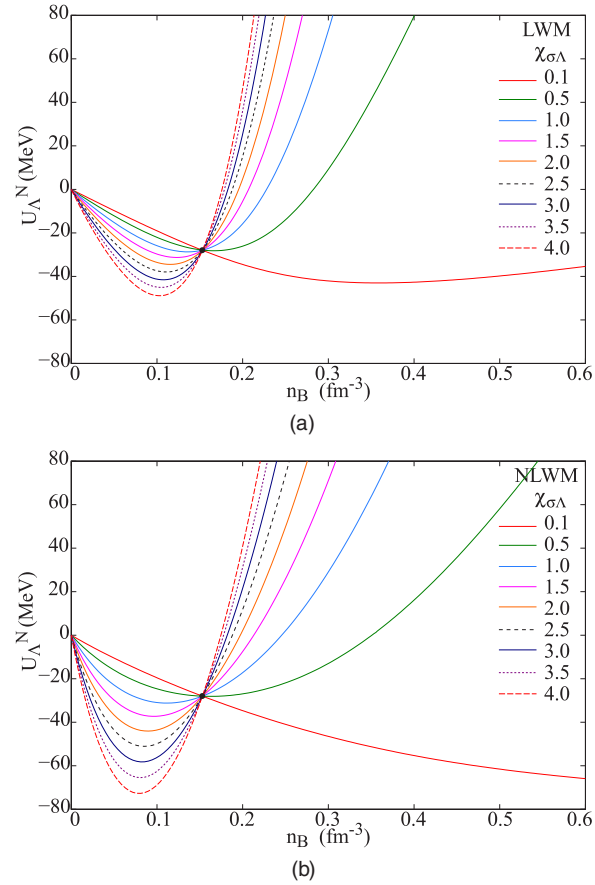

FIG. 2. U_Λ^N curves (constrained by data $U_\Lambda^N(n_0) = -28$ MeV, denoted by the black point) for some values of $\chi_{\sigma\Lambda}$ in (a) LWM and (b) NLWM.

we discuss the instabilities. A very similar reasoning without strange mesons was proposed in Ref. [36], where experimental values of the U_Λ^N were used to restrict the hyperon-meson coupling constants. In that paper, the resulting maximum stellar masses were also analyzed. Adding this condition

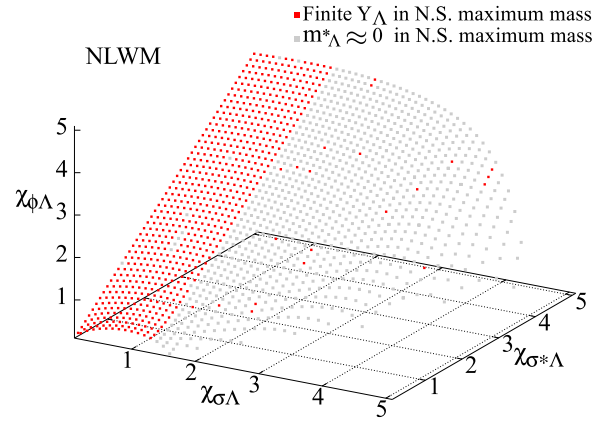

FIG. 3. Relations between parameters in the NLWM. 3D parameter space for for $\chi_{\phi\Lambda}$ constrained by the U_Λ^Λ potential. Gray points refer to parameters with which there is no numerical convergence in hyperonic stellar matter.

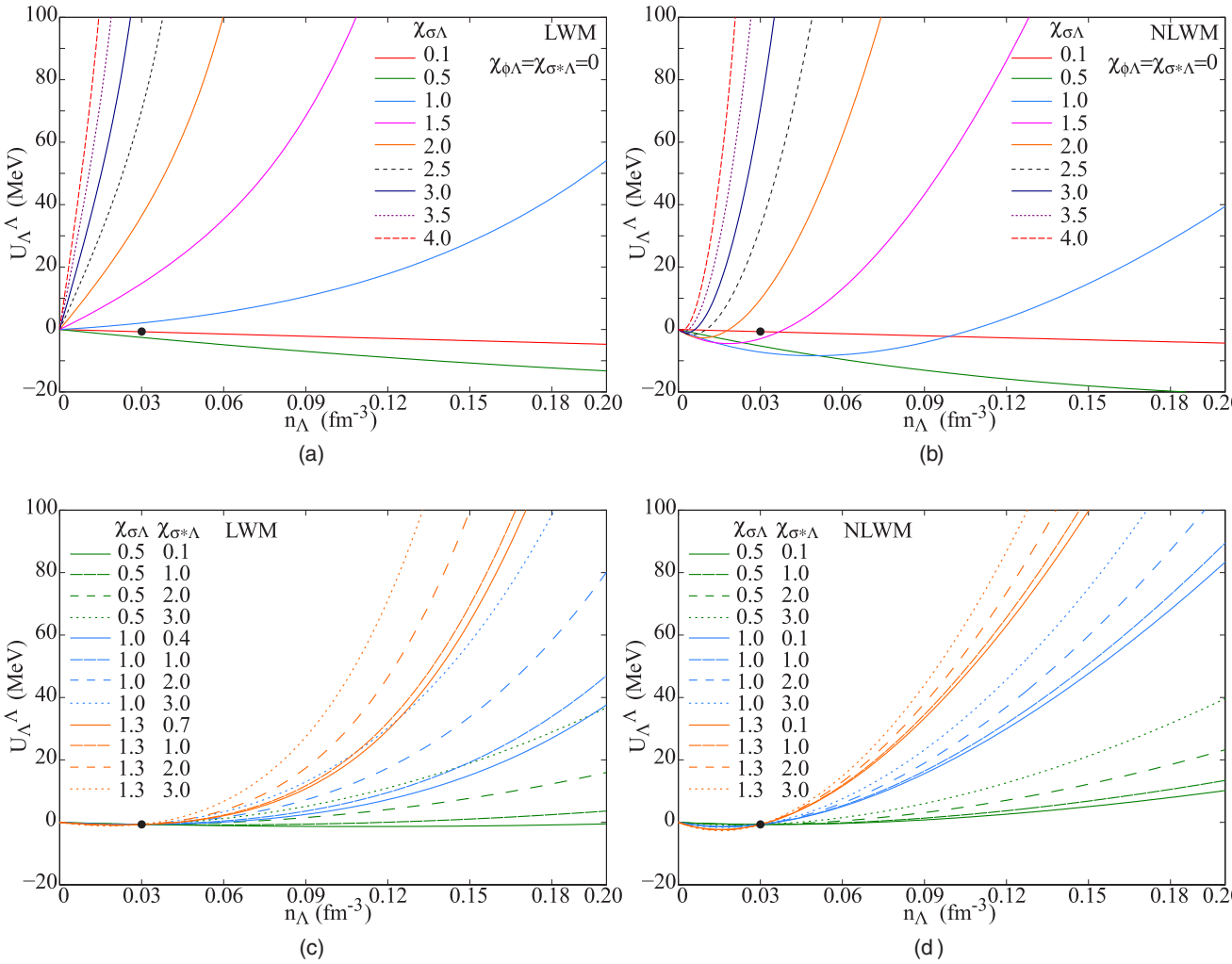

FIG. 4. The black points in each of these figures denote $U_\Lambda^\Lambda(n_0/5) = -0.67$ MeV. Panels (a) and (b) show the U_Λ^Λ potential without strange mesons for some values of $\chi_{\sigma\Lambda}$ in LWM and NLWM respectively. Panels (c) and (d) show U_Λ^Λ potential constrained to pass through the black point for some pairs of values of $\chi_{\sigma\Lambda}$ and $\chi_{\sigma^*\Lambda}$ in LWM and NLWM respectively.

still leaves us with a wide two-dimensional parameter space, which corresponds to an almost unconstrained model. A major simplification would be obtained if we do not introduce extra strange mesons. Indeed, if we put $\chi_{\phi\Lambda} = \chi_{\sigma^*\Lambda} = 0$ we are left with two equations and two unknowns, leading to a unique parameter choice for each of the models. This choice might sound appealing, especially if we recall that historically strange mesons were added [13] to provide extra binding in the Λ-Λ channel based on an analysis of hypernuclear data which nowadays appears questionable [31].

The families of U_Λ^Λ potential curves without strange mesons obtained with the LWM and the NLWM are shown in Figs. 4(a) and 4(b). We can see that the only possibility of having the very small extra binding suggested by experimental data, at the low densities explored in hypernuclei, is to have a potential which is unrealistically attractive at higher densities. This is due to the linear correlation between $\chi_{\sigma\Lambda}$ and $\chi_{\omega\Lambda}$ observed in Fig. 1. Consequently, the resulting EOS of stellar matter is clearly too soft. One can object that summarizing hypernuclear data to two values for the Λ potential in infinite matter is a very crude approximation, which is certainly true. However, it is well known from very different approaches that dedicated fits of hypernuclear data require some extra repulsion at higher density [10,68], in qualitative agreement with our oversimplified nuclear matter reasoning. This discussion implies that a realistic RMF model should probably include strange mesons, or alternatively more complex nonlinear couplings, even if this is done at the price of considerably enlarging the parameter space. In particular in this paper, our motivation being to extract a phase diagram as general as possible, we prefer considering a parameter space which is too large to one which is too narrow. We will therefore stick to the parameter space defined by Fig. 3.

Figures 4(c) and 4(d) display the LWM and NLWM U_Λ^Λ potential with the inclusion of strange mesons, and with the extra requirement of fulfilling Eq. (3.7). We can see that a wide range of behaviors is still possible. Figures 4(c) and 4(d) are globally similar, although in (d) the potential is slightly deeper than in (c) at very low density, i.e., $n_\Lambda < n_0/5$. For high densities, we can clearly see that all curves in Fig. 4(d)

are steeper than those in 4(c); i.e., for the parameters chosen, the U_Λ^Λ is more attractive with the NLWM than with the LWM. If one observes the values of the coupling constants, it is obvious that, as the $\chi_{\sigma\Lambda}$ and $\chi_{\sigma^*\Lambda}$ values related to the attractive interactions increase, so do the $\chi_{\omega\Lambda}$ and $\chi_{\phi\Lambda}$ values, related to the repulsive interaction.

IV. RESULTS FROM AFDMC

In recent years, *ab initio* models based on the Brueckner or Dirac-Brueckner theory [69–71] or on different quantum Monte Carlo simulation techniques [32,72–76] have been applied to (hyper)nuclear matter. Such models provide in the pure neutron sector—in the low -density regime where the underlying interactions are well known from scattering data, and three-body effects are not expected to be important—a very essential constraint to phenomenological mean field models, which starts to be routinely applied in order to fix some of the unknown couplings. Calculations including hyperons are still very scarce [32,69–71]. We here compare our results to the very recent AFDMC model [32], which has been satisfactorily compared to hypernuclear data [68] and allows producing very massive neutron stars in agreement with the observations [32], though with negligible strangeness fraction. This model is based on a phenomenological bare interaction inspired by the Argonne-Urbana forces [77], with the addition of a purely phenomenological three-body term. One of the advantages of the model is that the authors provide simple parametrizations of their numerical results for the neutron-Λ energy functionals, allowing both an easier comparison with our RMF results and a straigthforward calculation of the instability properties of hypermatter as predicted by an *ab initio* model. This latter point is discussed in the next section. The fit of the energy density of the neutron-Λ mixture is given by [32]

$$\epsilon_{\rm total}(n_n,n_\Lambda) = \left[a\left(\frac{n_n}{n_0}\right)^\alpha + b\left(\frac{n_n}{n_0}\right)^\beta\right]n_n + \frac{1}{2m_\Lambda}\frac{3}{5}n_\Lambda(3\pi^2 n_\Lambda)^{2/3} + (m_n n_n + m_\Lambda n_\Lambda) + c_1' n_\Lambda n_n + c_2' n_\Lambda n_n^2. \quad (4.1)$$

In this expression, the first term represents the energy density of pure neutron matter, where the parameters a, α, b, and β are listed in Table II and n_0 is the saturation point of symmetric nuclear matter. The second term highlights the kinetic energy density of pure Λ matter, and the last two terms, obtained from the fitting of the Monte Carlo results for different $Y_\Lambda = n_\Lambda/n_B$ fractions, provide an analytical parametrization for the difference between Monte Carlo energies of pure Λ and pure neutron matter. Notice that Λ-Λ interactions are neglected in Ref. [32], which explains why pure Λ matter ($n_n = 0$) behaves as a Fermi gas of noninteracting particles. This means that the extrapolations to high Λ densities have to be considered with a critical eye. The constants $c_1' \equiv c_1/n_0$ and $c_2' \equiv c_2/n_0^2$ with c_1 and c_2 are given in Table III. Using Eq. (4.1), the chemical potentials become

$$\mu_n(n_n) = a(\alpha+1)\left(\frac{n_n}{n_0}\right)^\alpha + b(\beta+1)\left(\frac{n_n}{n_0}\right)^\beta + m_n + c_1' n_\Lambda + 2c_2' n_\Lambda n_n, \quad (4.2)$$

and

$$\mu_\Lambda(n_\Lambda) = \frac{1}{2m_\Lambda}(3\pi^2 n_\Lambda)^{2/3} + m_\Lambda + c_1' n_n + c_2' n_n^2. \quad (4.3)$$

From thermodynamics we can also write the total pressure as follows:

$$p_{\rm total}(n_n,n_\Lambda) = \left\{\alpha a\left(\frac{n_n}{n_0}\right)^\alpha + \beta b\left(\frac{n_n}{n_0}\right)^\beta\right\}n_n + \frac{1}{5m_\Lambda}n_\Lambda \times\left(\frac{6\pi^2 n_\Lambda}{2s_\Lambda+1}\right)^{2/3} + c_1' n_n n_\Lambda + 2c_2' n_\Lambda n_n^2. \quad (4.4)$$

In Table III we show the sets of parameters proposed by the authors of Ref. [32] when only two-body forces are taken into account (ΛN), and also with the consideration of three-body forces that yield two different parametrizations ΛNN (I) and ΛNN (II). In the case of pure neutron matter, in the AFDMC approach the binding energy has no free parameters, and we can compare this result with the binding energy coming from our phenomenological RMF models. When we include a Λ fraction in the system, the *ab initio* model itself needs phenomenological inputs and is associated with theoretical error bars. This is due to the need of three-body forces in order to properly reproduce hypernuclear data [68]. The interval of predictions between ΛNN (I) and ΛNN (II), obtained using two different prescriptions for the three-body force, will be interpreted in the following as the present theoretical error bar on *ab initio* models, such that a phenomenological model like our RMF should lie between these two extreme cases.

TABLE II. Set of parameters used in the AFDMC *ab initio* model for PNM, from [32].

PNM	
n_0 (fm^{-3})	0.16
a (MeV)	13.4
α	0.514
b (MeV)	5.62
β	2.436

TABLE III. Set of parameters used in the *ab initio* AFDMC model including two- and three-body forces, from [32].

ΛN	
c_1 (MeV)	−71.0
c_2 (MeV)	3.7
$\Lambda N + \Lambda NN(I)$	
c_1 (MeV)	−77.0
c_2 (MeV)	31.3
$\Lambda N + \Lambda NN(II)$	
c_1 (MeV)	−70.0
c_2 (MeV)	45.3

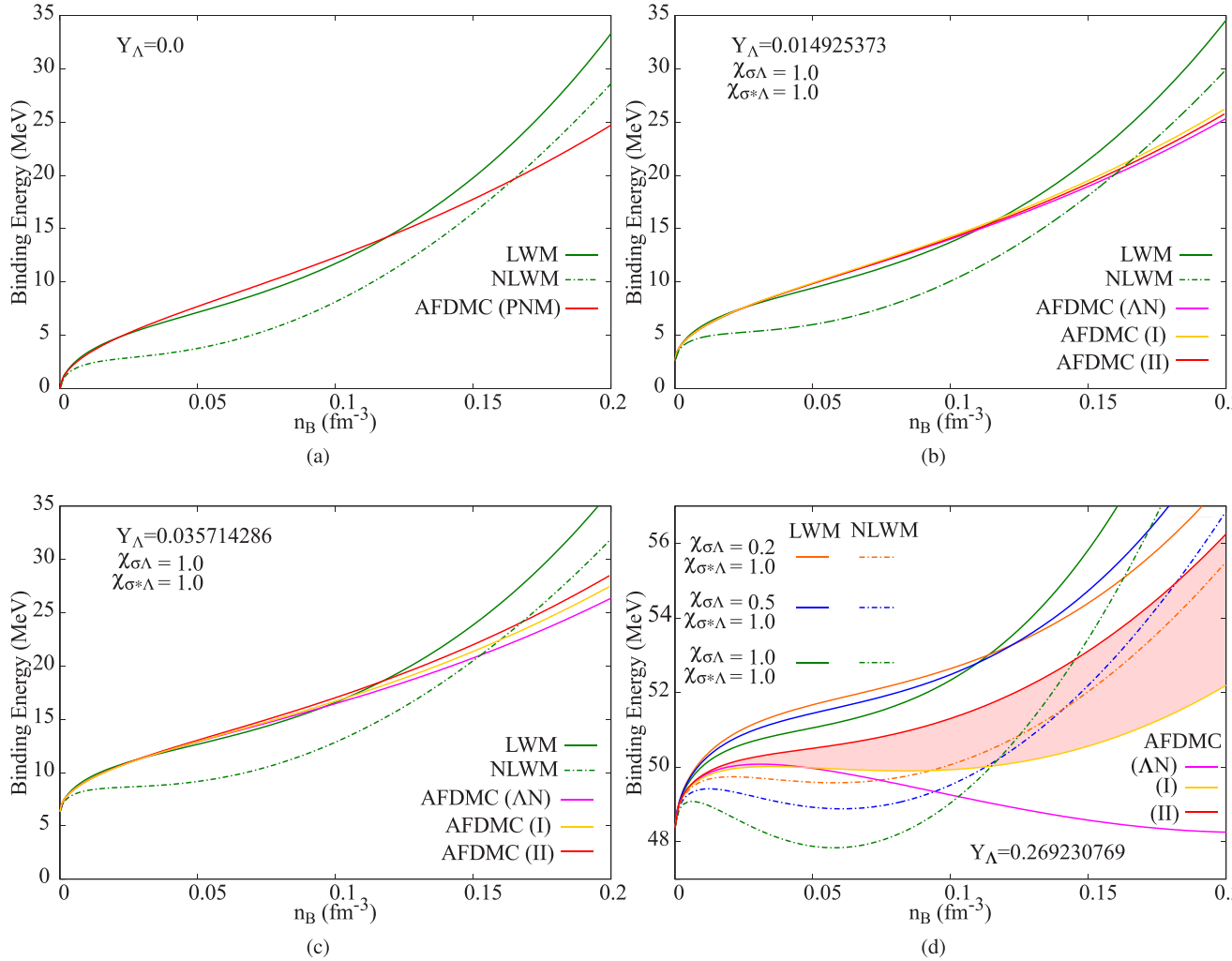

FIG. 5. Binding energy obtained with three different models, AFMDC, LWM, and NLWM, for different Λ fractions shown in (a)–(d).

In Fig. 5 we plot the binding energy for different values of the Λ fraction present in Ref. [32] for AFDMC and for representative RMF models. Figure 5(a) shows the binding energy for pure neutron matter. It has been known for a long time that RMF models are systematically too stiff at high neutron density in comparison to *ab initio* models. However, we can see that, for the subsaturation densities of interest for the present paper, the LWM agrees very well with the AFDMC, better than the NLWM, which in principle should be more sophisticated. This remains true for finite Λ fraction, as shown in Figs. 5(b) and 5(c), if this fraction is small enough. In this regime, the values of the Λ coupling do not play an important role, and the same level of reproduction is obtained for different choices of $\chi_{\sigma\Lambda}, \chi_{\sigma^*\Lambda}$.

The effect of three-body forces increases with increasing Λ fraction, and consequently the three versions of the AFDMC calculation start to considerably deviate from each other at the highest Λ fraction considered by the authors of [32] [Fig. 5(d)]. In this condition, the AFDMC (ΛN) becomes very bound, due to the attractive feature of the ΛN potential, while the three-body force in AFMDC (I) and (II) insures the necessary repulsion to sustain massive neutron stars. We can see that at high Λ fraction NLWM better reproduces the *ab initio* results, and the best reproduction is obtained for $\chi_{\sigma\Lambda} \ll \chi_{\sigma^*\Lambda}$. We have observed that U_Λ^Λ is more sensitive to changes in $\chi_{\sigma\Lambda}$ than $\chi_{\sigma^*\Lambda}$ as seen in Figs. 4(c) and 4(d). No matter how much we change these parameters, we do not notably change the degree of agreement between the RMF models and the AFDMC. In this sense the orange and green curves in Fig. 5(d) represent extreme choices for the RMF couplings in the two versions, LWM (full lines) and NLWM (dashed lines). To conclude, the inclusion of strange mesons is necessary to produce a RMF energy functional compatible with *ab initio* results at low baryonic density. For very low Λ fractions, as is the case in hypernuclei, the sensitivity to the Λ couplings is very small, and the LWM surprisingly leads to a very good agreement to the AFDMC parametrization. However, neither the linear nor the nonlinear version of the WM is satisfactory, if one wants to describe matter with a non-negligible proportion of Λ's, and a dedicated fit with density dependent couplings should be done to reduce the parameter space. For the purpose of the present paper we will continue with both models in our further analysis, keeping in mind that LWM results well reproduce *ab initio* pure neutron matter, while NLWM with

low values of $\chi_{\sigma\Lambda} \approx 0.2$–$0.5$ should give a reasonably realistic description of symmetric and asymmetric matter with an important contribution of strangeness.

V. SPINODAL AND CURVATURE MATRIX

In the present section we focus on the calculation of the instabilities in a system with neutrons, protons, and Λ's at $T = 0$ [64–67].

A first-order phase transition is signaled by an instability or concavity anomaly in the mean-field thermodynamic total energy density. The total energy density of a three-component system is a three-variable function of the densities. Therefore, we need to introduce the curvature matrix $\mathbf{C}$ associated with the scalar function ϵ at a point denoted by $P \in (n_n \times n_p \times n_\Lambda)$. Since our benchmark *ab initio* model only contains neutrons and Λ's, we consider first a two-component system case, where $P \in (n_n \times n_\Lambda)$, and later we comment about three-component systems [65,67] which are more relevant for hypernuclear physics. If ϵ is smooth, or at least twice continuously differentiable, $\mathbf{C}$ is symmetric. The curvature matrix elements are just second derivatives of the total energy density with respect to each independent variable. In our case the curvature matrix is just a 2×2 matrix with elements [78]

$$C_{ij} = \left(\frac{\partial^2 \epsilon(n_i, nj)}{\partial n_i \partial n_j} \right), \tag{5.1}$$

where $i, j = n, \Lambda$. As this matrix is self-adjoint, we can associate with it one bilinear form and one quadratic form at point P. So, the characteristic equation is

$$\mathtt{Det}(\mathbf{C} - \lambda \mathbf{1}_2) = 0, \tag{5.2}$$

where $\mathbf{1}_2$ is 2×2 identity matrix. In another way,

$$\lambda^2 - \mathtt{Tr}(\mathbf{C})\lambda + \mathtt{Det}(\mathbf{C}) = 0. \tag{5.3}$$

The eigenvalues and eigenvectors of $\mathbf{C}$ have geometric meaning if P is a critical point. We can solve their roots explicitly:

$$\lambda_1 = \tfrac{1}{2}(\mathtt{Tr}(\mathbf{C}) + \sqrt{\mathtt{Tr}(\mathbf{C})^2 - 4\mathtt{Det}(\mathbf{C})}) \tag{5.4}$$

and

$$\lambda_2 = \tfrac{1}{2}(\mathtt{Tr}(\mathbf{C}) - \sqrt{\mathtt{Tr}(\mathbf{C})^2 - 4\mathtt{Det}(\mathbf{C})}), \tag{5.5}$$

where $\mathtt{Det}(\mathbf{C}) = \lambda_1\lambda_2$ and $\mathtt{Tr}(\mathbf{C}) = \lambda_1 + \lambda_2$. The unitary eigenvectors are given by $\widehat{n}^1 = (\delta n_n^1, \delta n_\Lambda^1)$ and $\widehat{n}^2 = (\delta n_n^2, \delta n_\Lambda^2)$. For further analysis we define the direction by the ratios

$$\begin{aligned} \tan\theta_1 &= \frac{\delta n_\Lambda^1}{\delta n_n^1} = \frac{\lambda_1 - C_{nn}}{C_{n\Lambda}} \quad \text{and} \\ \tan\theta_2 &= \frac{\delta n_\Lambda^2}{\delta n_n^2} = \frac{\lambda_2 - C_{nn}}{C_{n\Lambda}}, \end{aligned} \tag{5.6}$$

where θ_1 and θ_2 are angles measured counterclockwise from the positive n_n axis. If P is a critical point and hence $\mathbf{C}$ is just a Hessian matrix so the determinant term is exactly the Gauss curvature and the trace is twice the mean curvature [78],

$$K = \lambda_1\lambda_2 \quad \text{and} \quad H = \tfrac{1}{2}(\lambda_1 + \lambda_2). \tag{5.7}$$

The stability properties of the system depend on the signs of the curvatures, K and H, at each point $P \in (n_n \times n_\Lambda)$ [5,7,64]:

(1) If $K > 0$ and $H > 0$, the system is stable.
(2) If $K > 0$ and $H < 0$, the system is unstable, both eigenvalues are negative, and two independent order parameters should be considered, meaning that more than two phases can coexist.
(3) If $K < 0$, the system is unstable, meaning that the order parameter of the transition is always one-dimensional, similar to the nuclear liquid-gas phase transition at subsaturation densities.
(4) If $K = 0$ and $H > 0$, the system is stable.
(5) If $K = 0$ and $H < 0$, the system is unstable.

In geometric terms the first and second conditions tell us that P represents an elliptic point, the third a hyperbolic point, and the fourth and fifth a parabolic point. For a three-component system we have to calculate numerically the equation

$$\mathtt{Det}(\mathbf{C} - \lambda \mathbf{1}_3) = 0, \tag{5.8}$$

where $\mathbf{1}_3$ is a 3×3 identity matrix. In terms of the polynomials,

$$\lambda^3 - \mathtt{Tr}(\mathbf{C})\lambda^2 + \tfrac{1}{2}[\mathtt{Tr}(\mathbf{C})^2 - \mathtt{Tr}(\mathbf{C}^2)]\lambda - \mathtt{Det}(\mathbf{C}) = 0, \tag{5.9}$$

where we have to analyze the signs of three eigenvalues. The remarkable feature of the liquid-gas phase transition is that one of all eigenvalues is negative, and the associated eigenvector gives the instability direction [67], which means that the energy surface is of a hyperbolic kind. Therefore, in the case of the simpler $n\Lambda$ system for a negative eigenvalue, the ratio (5.6) becomes

$$\frac{\delta n_\Lambda^-}{\delta n_n^-} = \frac{\lambda_- - C_{nn}}{C_{n\Lambda}}. \tag{5.10}$$

The next equation will be useful in the discussion about the ratio for $np\Lambda$ system with symmetric condition $n_n = n_p$:

$$\frac{\delta n_\Lambda^-}{\delta n_N^-} = \frac{\lambda_- - C_{NN}}{C_{N\Lambda}}. \tag{5.11}$$

From a physical viewpoint, the direction of instability defined by Eqs. (5.10) and (5.11) corresponds to the direction of spontaneous amplification of density fluctuations. In the case of the ordinary LG phase transition, it comes out that this direction is also very close to the direction of phase separation [5]. This is due to the short time scale associated with the spinodal dynamics. As a consequence, at any density point inside the spinodal, the density and composition of the two coexisting phases issued from the phase transition can be approximately inferred from the intersection of the unstable eigenvector direction and the spinodal contour.

In the next section we comment on our results.

VI. RESULTS

In order to understand the instabilities possibly present in the models discussed in Secs. III and IV, we need the analysis done in the preceding section. We have calculated the curvature matrix with the *ab initio* and RMF models. The whole density space is a three-dimensional space, and the spinodal region, when it occurs, is a three-dimensional volume

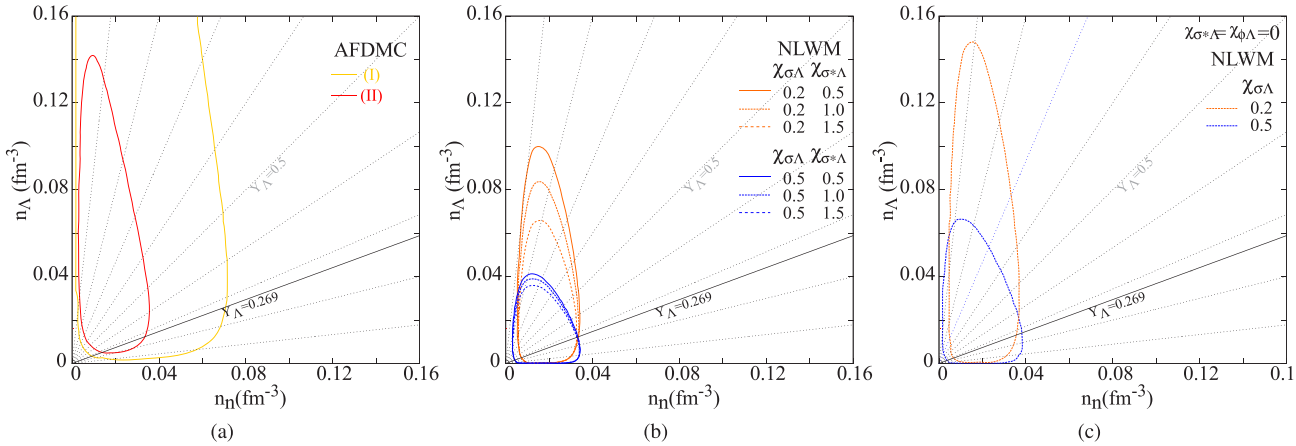

FIG. 6. Borders of the spinodal instability domains in the neutron and Λ density plane for AFMDC (left panel) with $\Lambda N + \Lambda NN$ (I) and $\Lambda N + \Lambda NN$ (II), and for NLWM with (central panel) and without (right panel) strange mesons.

that represents a geometric *locus* associated with the presence of at least one negative eigenvalue. It is well known that, in two-component systems with neutrons and protons, the liquid-gas phase transition occurs. The corresponding two-dimensional spinodal zone appears below the saturation density. So, in this system, one of the eigenvalues is negative. For a more complex system, with neutrons, protons and Λ's for example, we can fix the Λ-fraction to see how the two-dimensional spinodal region in the neutron-proton plane changes when Λ's are added. In all the models analyzed, for any proton fraction, and with all the different choices of couplings, we have systematically found one and only one negative eigenvalue in a finite-density space defining a spinodal region. The only exception is given by the $n\Lambda$ system studied with the LWM, which does not present any instability. However the instability is there in the *ab initio* model, and it appears in the LWM as soon as a non zero proton fraction is added to the system, meaning that the result of the LWM $n\Lambda$ mixture appears rather marginal.

Therefore we can conclude that a transition exists in the subsaturation nuclear matter including Λ hyperons, and this transition belongs to the liquid-gas universality class. In the following, we turn to study the characteristics of this transition in further detail.

In Fig. 6 we plot the spinodal areas in a system containing only neutrons and Λ's. In Fig. 6(a) two spinodal zones for the two different parametrizations of the *ab initio* model including three-body forces are shown. The behavior at high Λ density should be considered with caution, since the AFDMC calculations were only done for $Y_\Lambda < 0.269$. In Fig. 6(b), different spinodal zones are shown for the NLWM taking into account different values of the strange mesons coupling constants. Two more spinodal curves for neutron-Λ matter without strange mesons are also displayed in Fig. 6(c). Note that none of these shapes touch the horizontal or vertical axis, even if they look very close to the n_n axis for some of the models. This result is due to the fact that pure neutron and pure Λ matter are unbound. Indeed the spinodal instability at zero temperature leads to a phase transition where the system splits into two phases, the dense one representing the bound ground state. In the absence of a bound ground state, it is thus normal that the instability disappears. In the following, whenever the spinodal zone does not touch the axis it is clear that the reason underlying this behavior is an unbound system. It is interesting to observe that the widest extension of the instability is obtained with the most repulsive model.

This counterintuitive result probably stems from the fact that the highest repulsion at high density is correlated to a stronger attraction at low density also in the *ab initio* model. The behavior of the unstable eigenvector, shown in Figs. 7(a) and 7(b) for the two RMF parameter sets that better reproduce the *ab initio* EOS, is also interesting. We can see that it is close to the isoscalar direction $n_n + n_\Lambda$ as it is in the standard LG [7]. This simply means that the transition is between a dense and a diluted phase. In finite systems, the dense phase corresponds to a hypernucleus and the dilute phase to a (hyper)gas (which at $T = 0$ corresponds to zero density, and which would exist and would be in equilibrium with the hypernucleus at finite temperature). Figure 7(c) shows the ratio $\delta n_\Lambda^- / \delta n_n^-$ as a function of Y_Λ for some couplings and baryon densities for $Y_p = 0.0$. We can see that, for very low Λ fractions, the direction of phase separation is steeper than the constant Λ-fraction line. This means that the dense phase is more symmetric than the dilute phase. We also depict the line that represents n_Λ / n_n, so that it becomes visually easy to compare it with the direction of the eigenvectors.

The instability direction can be better spotted from Fig. 7(c), which displays the unstable eigenvector as a function of the Λ fraction. We can see that the instability eigenvectors are almost independent of the baryonic density. This means that the proportion of Λ in the dense phase following the spinodal decomposition is the same whatever the timescales and dynamics in the spinodal zone, and is well defined by the direction of the instability eigenvectors. This proportion monotonically increases with the Λ fraction, but never reaches equality between neutrons and Λ. This feature is due to the mass difference between the two baryonic species, as well as to the reduced attraction in the Λ channel. It is at variance with the ordinary nuclear liquid-gas which is associated with the fractionation or distillation phenomenon [3,7], with the dense phase being systematically more symmetric than the dilute

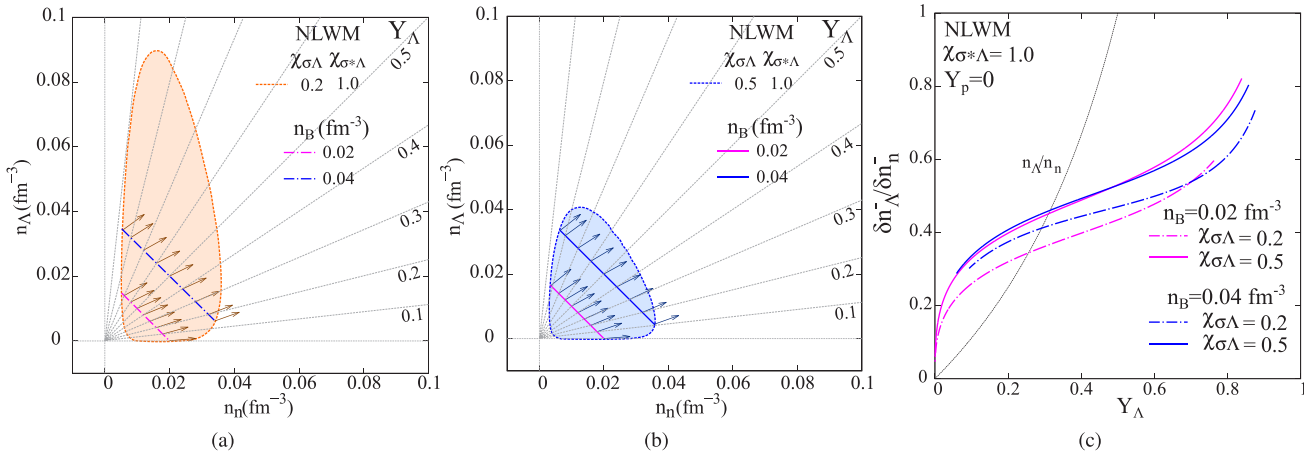

FIG. 7. Spinodal instability domains in the neutron and Λ density plane with eigenvectors for NLWM. From (a) to (b) we vary $\chi_{\sigma\Lambda}$ with fixed $\chi_{\sigma^*\Lambda} = 1.0$. (c) Ratio $\delta n_\Lambda^-/\delta n_n^-$ as a function of the Y_Λ for some couplings and baryon densities for $Y_p = 0.0$.

phase (see Fig. 9). The optimal proportion of Λ increases with increasing scalar coupling, as can be intuitively expected.

Now we would like to see how this affects the spinodal zone calculations in the three-component system, which is more relevant for nuclear physics applications. Figure 8 shows the three-dimensional spinodal volumes for particular cases: $\chi_{\sigma\Lambda} = 0.2$ and $\chi_{\sigma^*\Lambda} = 1.0$ in the NLWM. The behavior shown in both figures does not depend on the couplings used. The general pattern is always the same. In Fig. 8(a) the blue contour and dots are the surface of the spinodal volume and the red shapes mean the slices in the orthogonal planes of this volume. Shape 1 represents the neutron-Λ spinodal area, 2 th proton-Λ spinodal area, and 3 the neutron-proton spinodal area. The red dashed curve 4 shows the vertical plane that cuts the volume passing by $n_n = n_p$. Figure 8(b) is similar to 8(a), but in this case the black dashed lines represent constant Y_Λ cuts. $Y_\Lambda = 0.5$ is the special value we choose for further analysis and is highlighted in red.

Analogous pictures for the LWM are quite similar, apart from the fact that the size is a little bigger and no instability regions exist for (n,Λ) and (p,Λ) systems. Hence, in the following when we report different cuts of three-dimensional spinodal picture in RMF models, we assume that Fig. 8 is useful to illustrate the cases using LWM and NLWM.

A first interesting cut is at constant Λ fraction, because it leads to the same representation as for the usual LG phase transition, which is obtained in the limit $Y_\Lambda = 0$. This is done in Fig. 9, which shows the spinodal region in the neutron-proton plane obtained with the NLWM model. It is important to remark that only NLWM gives reasonable properties for symmetric matter in the absence of hyperons, and for LWM we omitted the corresponding results here. Figure 9(a) shows the NLWM spinodal for $Y_\Lambda = 0$ and corresponding eigenvectors that define the region of instability, analogous to the one represented by shape (3) in Fig. 8(a). In Fig. 9(b) the ratios $\delta n_p^-/\delta n_n^-$ are plotted as a function of the proton fraction for the same fixed baryon densities shown in Fig. 9(a).

In Fig. 10(a) the gray curve is the frontier of the spinodal for $Y_\Lambda = 0.0$ and the colored curves are the spinodal frontiers obtained for $Y_\Lambda = 0.5$ and different strange meson coupling

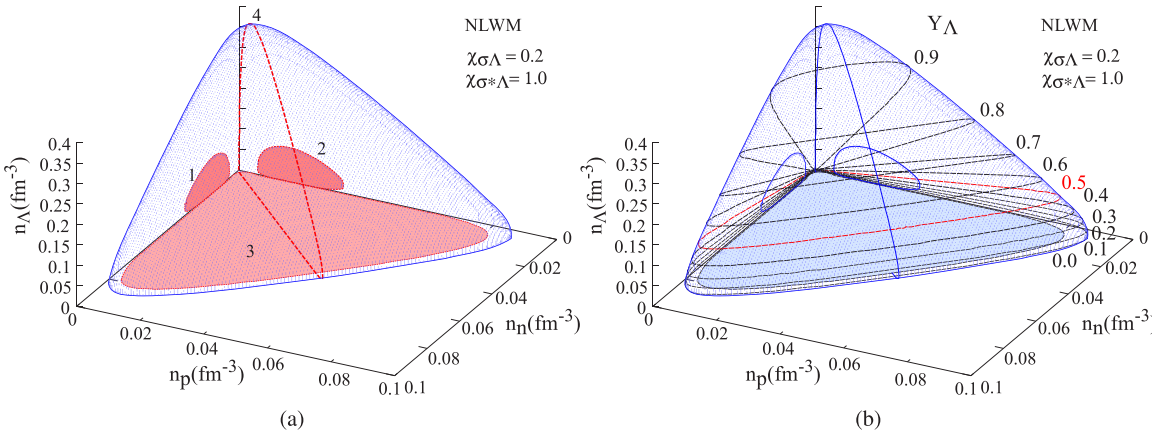

FIG. 8. Three-dimensional spinodal surfaces in the NLWM for a particular choice of coupling constrained parameters. In (a) the numbers denote cuts on the surface: (1) neutron-Λ spinodal area, (2) proton-Λ spinodal area, (3) neutron-proton spinodal area, and (4) the frontier of the spinodal area when we cut the three-dimensional spinodal volume by a vertical plane passing by $n_n = n_p$. Panel (b) shows the slices when we fix Y_Λ; the red shaded one is a special case.

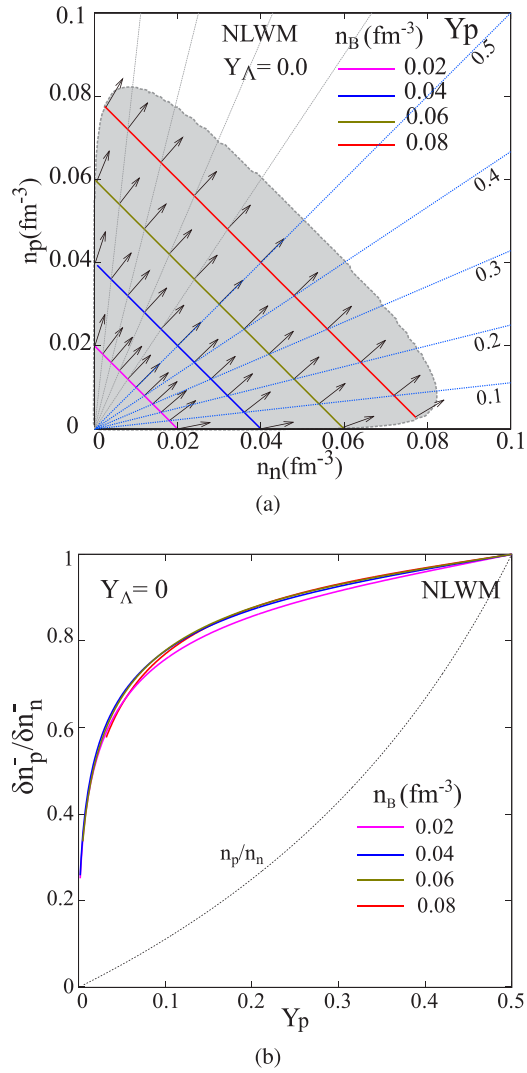

FIG. 9. (a) Spinodal for neutron-proton matter with eigenvectors in NLWM. (b) The ratio $\delta n_p^-/\delta n_n^-$ plotted as a function of the proton fraction for $Y_\Lambda = 0$.

constants in the NLWM. These colored shapes are the projections of the spinodal curves in the neutron-proton plane for $Y_\Lambda = 0.5$ [see Fig. 8(b)]. We recall from Sec. IV that at low density the LWM is more realistic for the case $Y_\Lambda = 0$ (left side), while the NLWM is in better agreement with the *ab initio* model for important Λ fractions (right side). In any case we can see that the phase diagrams of the two models are very similar, the NLWM instability zone being only slightly narrower.

Panels (a) and (b) of Fig. 9 recall the usual characteristics of the nuclear liquid-gas phase transition [5,7]. As is well known, the instability covers a huge part of the subsaturation region and has an essentially isoscalar character. The instability eigenvectors point toward a direction which is intermediate between the isoscalar direction (observed only for symmetric matter $n_n = n_p$) and the direction of constant isospin. As a consequence, the dense phase is systematically more symmetric than the dilute phase. Indeed, at zero temperature the dilute phase is a pure gas of neutrons (protons) if the system is neutron (proton) rich [7]. From panels (a) and (c) of Fig. 10 we additionally learn that the LG instability is clearly preserved by the addition of strangeness. However, the transition is quenched for strongly coupled hyperons. Indeed, we can clearly see that when $\chi_{\sigma\Lambda}$ increases the spinodal area decreases. Considering that the most realistic value lies around $\chi_{\sigma\Lambda} \approx 0.2$–$0.5$, this quenching is small. On the other side, when $\chi_{\sigma^*\Lambda}$ increases, the modification of the spinodal is very small. This is expected, since the strange mesons are only coupled to strange baryons and are therefore expected to affect essentially the Λ density, which is not represented here. Due to the weak effect of $\chi_{\sigma^*\Lambda}$ in the spinodal frontier, we select the value $\chi_{\sigma^*\Lambda} = 1.0$ to study the eigenvectors in the neutron-proton plane displayed in the next figures. For the NLWM spinodal area shown in Fig. 10(b), the vectors represent the projection of the instability eigenvectors on the neutron-proton plane. In Fig. 10(c) the ratios $\delta n_p^-/\delta n_n^-$ are plotted as a function of the proton fraction. No difference can be seen with respect to the normal LG: whatever the percentage

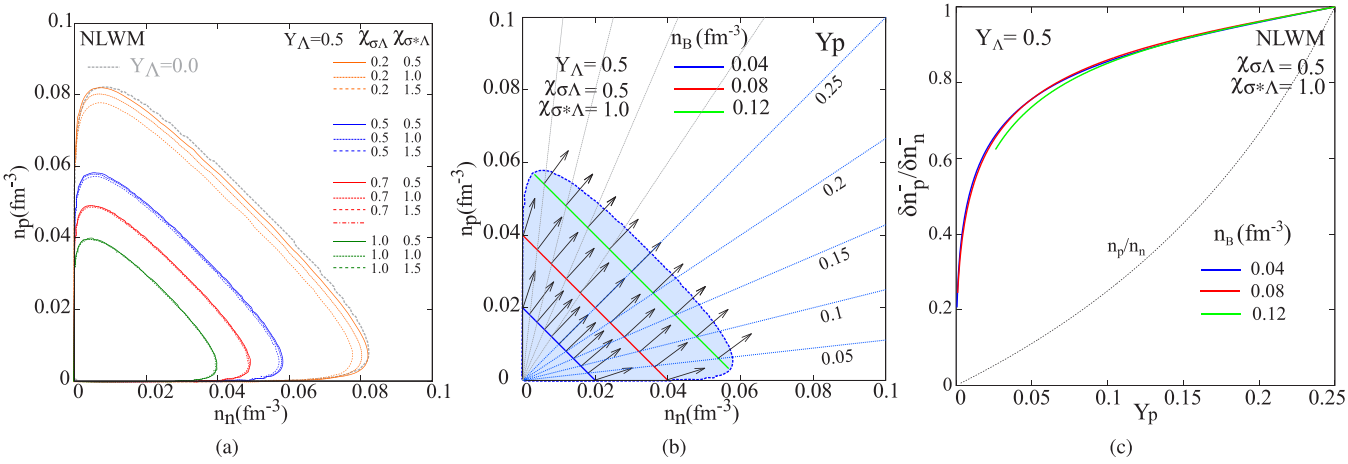

FIG. 10. (a) Spinodal frontiers in the neutron and proton density plane for $Y_\Lambda = 0.0$ and $Y_\Lambda = 0.5$ and several sets of coupling constants in NLWM. (b) Frontier of the spinodal instability domain of the (n, p, Λ) mixture with $Y_\Lambda = 0.5$ for $\chi_{\sigma\Lambda} = 0.5$ and $\chi_{\sigma^*\Lambda} = 1.0$ with eigenvectors in NLWM. (c) The ratio $\delta n_p^-/\delta n_n^-$ plotted as a function of the proton fraction. The isospin ratio n_p/n_n is also represented.

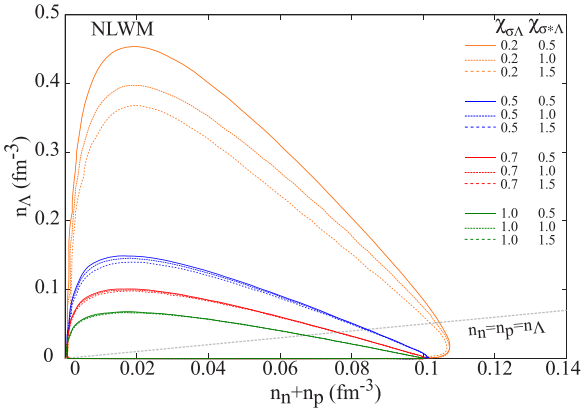

FIG. 11. Spinodal in the nucleon and Λ density plane (keeping $n_n = n_p$). Colors contours are sliced shapes from the 3D spinodal in density space and varying $\chi_{\sigma\Lambda}$ and $\chi_{\sigma^*\Lambda}$ in NLWM. The gray dotted line represents the $n_N = n_\Lambda$ line.

of Λ's, the neutron-proton composition of the dense phase (i.e., the hypernucleus) is unmodified, even if the density is reduced.

This finding might seem in contradiction with recent studies in multiply strange hypernuclei [22–24], where it is seen that the driplines are modified by the Λ fraction. However, these modifications are essentially due to shell and Coulomb effects, which are not accounted for in this infinite-matter calculation. If we change our perspective from the neutron-proton plane to imagine the general three-dimensional spinodal *locus,* and instead of fixing Y_Λ, as before, we fix the symmetric matter condition $n_N = 2n_n = 2n_p$, the resulting plane slice crossing this three-dimensional volume is similar to the curve denoted by number 4 in Fig. 8(a). The related spinodal areas for the NLWM and many choices of the coupling parameters are shown in Fig. 11.

The comparison to the *ab initio* model of Sec. IV suggests that the most realistic phase diagram should be between the ones corresponding to $\chi_{\sigma\Lambda} = 0.2$ and 0.5, which gives an energy functional intermediate between the two AFDMC parametrizations of three-body forces. We can see that the coupling to the strange meson $\chi_{\sigma^*\Lambda}$ has a bigger effect in this plane as expected. Still, its influence on the spinodal is small. This means that the wide uncertainty on the strange mesons has a negligible influence on the phase transition. The biggest uncertainty concerns the extension of the spinodal zone along the n_Λ axis. It is, however, important to stress that this situation $n_N < n_\Lambda < n_0$ does not correspond to any known physical system. Every shape shown touches the horizontal axis when $Y_p = 0.5$, as should occur considering that the np system is bound. At this point we can refer to Fig. 3 to see that our restriction of $\chi_{\sigma\Lambda}$ does not affect much the spinodal zone analysis, because when we increase $\chi_{\sigma\Lambda}$ up to 1.3 the spinodal zone tends to become flatter in the Λ-density direction. Even if the calculation might be not realistic for very high Λ fraction, we can conclude that the LG phase transition is still present in multistrange systems.

Finally, Figs. 12(a) and 12(b) show the projections of the instability eigenvectors in the nucleon and Λ density plane. We can see that a non-negligible component of the order parameter lies along the n_Λ direction, meaning that the Λ density is an order parameter of the phase transition, or in other words that the dense phase is also the phase with the higher strangeness content. These eigenvectors are almost parallel to each other, and considerably deviate with respect to the direction of the constant Λ-fraction lines as seen in Fig. 12(c). Interestingly, in a large portion of the spinodal zone the instability direction is approximately constant, $\delta n_\Lambda^-/\delta n_N^- \approx 0.2$, for both parameter sets. Only for very small and very high Λ fraction is a deviation observed, which is expected because by construction the instability must tend toward the nonstrange direction in the absence of strangeness.

We recall that the direction of instability can be used as an approximate estimator of the density and composition of the two coexisting phases issued from the phase transition. In particular, since the gas density is always much smaller than the density of the liquid, we can infer the composition of the dense (L) phase as $n_\Lambda^L/n_N^L \approx \delta^- n_\Lambda/\delta^- n_N$. We can see that, in the case of the N-Λ phase diagram, the instability points toward an "optimal" composition $n_\Lambda^L \approx 0.2 n_N^L$, whatever the

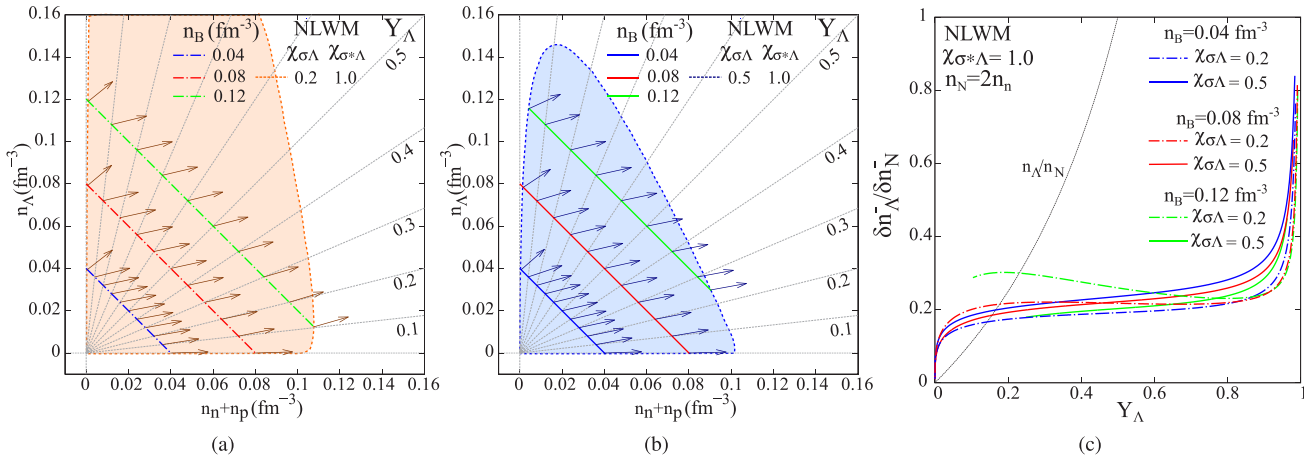

FIG. 12. Spinodals in nucleon and Λ density plane ($n_n = n_p$) with eigenvectors in NLWM. From (a) to (b) we vary $\chi_{\sigma\Lambda}$ with fixed $\chi_{\sigma^*\Lambda} = 1.0$. (c) Ratio $\delta n_\Lambda^-/\delta n_N^-$.

baryonic density, coupling constants, and Λ fraction. It will be very interesting to verify if such an optimal composition is obtained in calculations of multiple-strange hypernuclei. As in the case of the simpler n-Λ system, the fact that the instability always points toward Λ-poor systems is at variance with the distillation phenomenon, characteristic of the fluid and nuclear LG phase transition with more than one component [3,7]. In a one-component-like thermodynamics, which occurs in the case of classical indistinguishable particles with identical couplings, the direction of phase separation is given by the constant composition line (here, $Y_\Lambda = \text{const}$). In the case of distillation, the direction is tilted toward the isoscalar direction corresponding to equal composition. This happens in simple fluids when isovector couplings are more attractive than isoscalar ones [79,80], and in the proton-neutron system, even without any isospin breaking effect, because of the fermionic nature of the particles [7]. In this exotic mixture, neither of the two situations applies. The symmetry breaking between nucleons and Λ's comes from the difference in the bare mass of the particles and the less attractive couplings. Still, for low-Λ fractions $Y_\Lambda \leqslant 0.2$, the direction of phase separation is steeper than the constant-Λ-fraction line. This means that the dense phase is more symmetric than the dilute phase. This thermodynamic finding is compatible with the observation in Ref. [25] that the Λ's produced in heavy-ion collisions should stick to the clusters (i.e., the dense phase) rather than being emitted as free particles (i.e., the gas).

VII. SUMMARY AND CONCLUSIONS

We have investigated the phase diagram at subsaturation density, for baryonic matter including neutrons, protons, and Λ hyperons, within a RMF approach. For the nucleonic EOS, we have considered the GM1 parametrization of NLWM, together with the simpler LWM. Strange mesons were included to allow a wide exploration of the possible phenomenology for the (still largely unknown) hyperon-nucleon and hyperon-hyperon couplings, with minimal requirements on the potential depths extracted from hypernuclear data. Imposing these requirements leads to a strong linear correlation between the attractive and the repulsive couplings, for both the normal and the strange mesons. These constraints leave us with a two-dimensional parameter space, which we have varied widely in order to pin down generic features of the phase diagram.

Our main focus was the understanding of the instabilities in the hypernuclear matter, and specifically the influence of Λ's in the well known liquid-gas phase transition of nuclear matter. The existence of an instability as a signature of a first-order phase transition was identified by analyzing the curvature of the thermodynamic potential with respect to the nucleonic and strange densities. In all our studies, one and only one negative eigenvalue has been found, showing that the phase transition still exists in the presence of strangeness and is still of LG type, even if its extension in the density space shrinks with increasing strangeness. The negative eigenvalue corresponds to the direction in density space, in which density fluctuations get spontaneously and exponentially amplified in order to achieve phase separation. This eigenvalue is seen to systematically have a non-negligible component in the direction of the strange density. This means that strangeness can be viewed as an order parameter of the transition.

Less expected is the fact that the instability direction systematically points to an almost fixed proportion of Λ's in the dense phase, at variance with the phenomenon of distillation typical of binary mixtures. This proportion was of the order of 20% in the models we considered; this means that, in a dilute system with a small contribution of Λ's, these Λ's will preferentially belong to the dense clusterized phase. These conclusions are general and appear largely model independent. In contrast, the specific shape of the phase diagram would obviously depend on the choice of the free $\chi_{\sigma^*\Lambda}$ and $\chi_{\phi\Lambda}$ couplings. Some hints of a more quantitative estimation of the thermodynamics were obtained from the analysis of the simpler $n\Lambda$ phase diagram extracted from the *ab initio* AFDMC calculation of Ref. [32]. The characteristics of the phase transition are confirmed in the *ab initio* model, even if the phase diagram extension depends on the three-body force model in an important way.

The comparison of the RMF with the AFDMC also reveals some limitations of the phenomenological model at low density. Indeed the popular GM1 model is shown to compare very poorly to the *ab initio* calculation of pure neutron matter, even at the low densities considered in the present study. Unexpectedly, the simpler LWM is in very good agreement with the *ab initio* predictions at low density. Concerning the $n\Lambda$ mixture, the energy functional is within the theoretical error bars if $0.2 \leqslant \chi_{\sigma\Lambda} < 0.5$. Other parametrizations could change the quantitative results that we have presented in this paper. In particular, a recent work [81] shows that the scalar-isovector δ meson also plays an important role in satisfying both nuclear bulk and stellar properties constraints. The use of another parameter set and/or the inclusion of this new degree of freedom requires a complete calculation from the very beginning because the nucleon-Λ potential, Eq. (3.3), has to be readjusted. However, the qualitative results will be certainly similar, since the whole 3D parameter space associated with strangeness was spanned. As a perspective for future work, it will be very interesting to analyze the instability behavior of a density-dependent coupling RMF model, directly fitted to the *ab initio* calculation.

ACKNOWLEDGMENTS

This work was partially supported by CAPES/COFECUB project 853/15 and CNPq under grants 300602/2009-0 and 470366/2012-5.

[1] J. E. Finn *et al.*, Phys. Rev. Lett. **49**, 1321 (1982).
[2] G. Bertsch and P. J. Siemens, Phys. Lett. B **126**, 9 (1983).
[3] H. Müller and B. D. Serot, Phys. Rev. C **52**, 2072 (1995).
[4] N. K. Glendenning, Phys. Rep. **342**, 393 (2001).

[5] J. Margueron and P. Chomaz, Phys. Rev. C **67**, 041602 (2003); P. Chomaz, M. Colonna, and J. Randrup, Phys. Rep. **389**, 263 (2004).
[6] C. B. Das *et al.*, Phys. Rep. **406**, 1 (2005).
[7] C. Ducoin, Ph. Chomaz, and F. Gulminelli, Nucl. Phys. A **771**, 68 (2006).
[8] A. Carbone, A. Polls, A. Rios, and I. Vidaña, Phys. Rev. C **83**, 024308 (2011).
[9] C. Wellenhofer, J. W. Holt, and N. Kaiser, Phys. Rev. C **92**, 015801 (2015).
[10] D. J. Millener, C. B. Dover, and A. Gal, Phys. Rev. C **38**, 2700 (1988).
[11] J. Mareš and J. Žofka, Z. Phys. A **333**, 209 (1989).
[12] M. Rufa, J. Schaffner, J. Maruhn, H. Stöcker, W. Greiner, and P.-G. Reinhard, Phys. Rev. C **42**, 2469 (1990).
[13] J. Schaffner, C. B. Dover, A. Gal *et al.*, Ann. Phys. (NY) **235**, 35 (1994).
[14] J. Schaffner-Bielich, M. Hanauske, H. Stocker, and W. Greiner, Phys. Rev. Lett. **89**, 171101 (2002).
[15] V. Dexheimer and S. Schramm, Astrophys. J. **683**, 943 (2008).
[16] S. Aoki *et al.*, Prog. Theor. Phys. **85**, 1287 (1991).
[17] C. B. Dover, D. J. Millener, A. Gal, and D. H. Davis, Phys. Rev. C **44**, 1905 (1991).
[18] S. Aoki *et al.*, Nucl. Phys. A **828**, 191 (2009).
[19] J. K. Ahn *et al.*, Phys. Rev. C **88**, 014003 (2013).
[20] J. Schaffner-Bielich, Nucl. Phys. A **804**, 309 (2008).
[21] F. Minato and K. Hagino, Phys. Rev. C **88**, 064303 (2013).
[22] M. Ikram, S. K. Singh, A. A. Usmani, and S. K. Patra, Int. J. Mod. Phys. E **23**, 1450052 (2014).
[23] H. Y. Sang, X. S. Wang, J. H. Wang, and H. F. Lü, Eur. Phys. J. A **50**, 52 (2014).
[24] E. Khan, J. Margueron, F. Gulminelli, and Ad. R. Raduta, Phys. Rev. C **92**, 044313 (2015).
[25] S. Mallik and G. Chaudhuri, Phys. Rev. C **91**, 054603 (2015).
[26] J. Schaffner and I. N. Mishustin, Phys. Rev. C **53**, 1416 (1996).
[27] S. Weissenborn, D. Chatterjee, and J. Schaffner-Bielich, Nucl. Phys. A **881**, 62 (2012).
[28] S. Weissenborn, D. Chatterjee, and J. Schaffner-Bielich, Phys. Rev. C **85**, 065802 (2012).
[29] Luiz L. Lopes and Debora P. Menezes, Phys. Rev. C **89**, 025805 (2014).
[30] M. E. Gusakov, P. Haensel, and E. M. Kantor, Mon. Not. R. Astron. Soc. **439**, 318 (2014).
[31] H. Shen, F. Yang, and H. Toki, Prog. Theor. Phys. **115**, 325 (2006).
[32] D. Lonardoni, A. Lovato, S. Gandolfi, and F. Pederiva, Phys. Rev. Lett. **114**, 092301 (2015).
[33] M. H. Johnson and E. Teller, Phys. Rev. **98**, 783 (1955); H. P. Duerr, *ibid.* **103**, 469 (1956); J. D. Walecka, Ann. Phys. (N.Y.) **83**, 491 (1974).
[34] J. Boguta and A. R. Bodmer, Nucl. Phys. A **292**, 413 (1977).
[35] N. K. Glendenning, Phys. Lett. B **114**, 392 (1982).
[36] N. K. Glendenning, Astrophys. J. **293**, 470 (1985).
[37] B. D. Serot and J. D. Walecka, Adv. Nucl. Phys. **16**, 1 (1986).
[38] B. D. Serot and H. Uechi, Ann. Phys. (NY) **179**, 272 (1987).
[39] N. K. Glendenning, *Compact Stars*, 2nd ed. (Springer, New York, 2000).
[40] J. Ellis, J. I. Kapusta, and K. A. Olive, Nucl. Phys. B **348**, 345 (1991).
[41] J. Boguta and S. Bohrmann, Phys. Lett. B **102**, 93 (1981).
[42] M. Rufa *et al.*, J. Phys. G **13**, L143 (1987).
[43] A. Taurines *et al.*, Mod. Phys. Lett. A **15**, 1789 (2000).
[44] A. Pais, Rev. Mod. Phys. **38**, 215 (1966).
[45] Z. S. A. Moszkowski, Phys. Rev. D **9**, 1613 (1974).
[46] S. Pal, M. Hanauske, I. Zakout, H. Stöcker, and W. Greiner, Phys. Rev. C **60**, 015802 (1999).
[47] S. Banik, M. Hempel, and D. Bandyopadhyay, Astrophys. J. Suppl. **214**, 22 (2014).
[48] T. Miyatsu, M.-K. Cheoun, and K. Saito, Phys. Rev. C **88**, 015802 (2013).
[49] N. K. Glendenning and S. A. Moszkowski, Phys. Rev. Lett. **67**, 2414 (1991).
[50] N. K. Glendenning, Phys. Rev. C **64**, 025801 (2001).
[51] S. Marcos, R. J. Lombard, and J. Mareš, Phys. Rev. C **57**, 1178 (1998).
[52] E. N. E. van Dalen, G. Colucci, and A. Sedrakian, Phys. Lett. B **734**, 383 (2014).
[53] G. Colucci and A. Sedrakian, Phys. Rev. C **87**, 055806 (2013).
[54] P. H. Pile, S. Bart, R. E. Chrien, D. J. Millener, R. J. Sutter, N. Tsoupas, J.-C. Peng, C. S. Mishra, E. V. Hungerford, T. Kishimoto, L.-G. Tang, W. vonWitsch, Z. Xu, K. Maeda, D. Gill, R. McCrady, B. Quinn, J. Seydoux, J. W. Sleight, R. L. Stearns, H. Plendl, A. Rafatian, and J. Reidy, Phys. Rev. Lett. **66**, 2585 (1991); T. Hasegawa, O. Hashimoto, S. Homma, T. Miyachi, T. Nagae, M. Sekimoto, T. Shibata, H. Sakaguchi, T. Takahashi, K. Aoki, H. Noumi, H. Bhang, M. Youn, Y. Gavrilov, S. Ajimura, T. Kishimoto, A. Ohkusu, K. Maeda, R. Sawafta, and R. P. Redwine, Phys. Rev. C **53**, 1210 (1996); H. Hotchi, T. Nagae, H. Outa, H. Noumi, M. Sekimoto, T. Fukuda, H. Bhang, Y. D. Kim, J. H. Kim, H. Park, K. Tanida, O. Hashimoto, H. Tamura, T. Takahashi, Y. Sato, T. Endo, S. Satoh, J. Nishida, T. Miyoshi, T. Saitoh, T. Kishimoto, A. Sakaguchi, S. Ajimura, Y. Shimizu, T. Mori, S. Minami, M. Sumihama, R. Sawafta, and L. Tang, *ibid.* **64**, 044302 (2001).
[55] I. Vidana, A. Polls, A. Ramos, and H.-J. Schulze, Phys. Rev. C **64**, 044301 (2001).
[56] B. Bhowmick, A. Bhattacharyya, and G. Gangopadhyay, Int. J. Mod. Phys. E **21**, 1250069 (2012).
[57] H. Takahashi *et al.*, Phys. Rev. Lett. **87**, 212502 (2001).
[58] K. Nakazawa, Nucl. Phys. A **835**, 207 (2010).
[59] A. Rabhi, C. Providência, and J. Da Providência, Phys. Rev. C **79**, 015804 (2009).
[60] C. Providência, L. Brito, S. S. Avancini, D. P. Menezes, and Ph. Chomaz, Phys. Rev. C **73**, 025805 (2006).
[61] S. S. Avancini, L. Brito, D. P. Menezes, and C. Providência, Phys. Rev. C **70**, 015203 (2004).
[62] C. Ducoin, C. Providência, A. M. Santos, L. Brito, and Ph. Chomaz, Phys. Rev. C **78**, 055801 (2008).
[63] S. S. Avancini, L. Brito, Ph. Chomaz, D. P. Menezes, and C. Providência, Phys. Rev. C **74**, 024317 (2006).
[64] F. Gulminelli, Ad. R. Raduta, and M. Oertel, Phys. Rev. C **86**, 025805 (2012).
[65] F. Gulminelli, Ad. R. Raduta, M. Oertel, and J. Margueron, Phys. Rev. C **87**, 055809 (2013).
[66] A. R. Raduta, F. Gulminelli, and M. Oertel, arXiv:1406.0395.
[67] M. Oertel, C. Providência, F. Gulminelli, and Ad. R. Raduta, J. Phys. G: Nucl. Part. Phys. **42**, 075202 (2015).
[68] D. Lonardoni, F. Pederiva, and S. Gandolfi, Phys. Rev. C **89**, 014314 (2014).
[69] G. F. Burgio, H.-J. Schulze, and A. Li, Phys. Rev. C **83**, 025804 (2011).

[70] H.-J. Schulze and T. Rijken, Phys. Rev. C **84**, 035801 (2011).
[71] T. Katayama and K. Saito, Phys. Lett. B **747**, 43 (2015).
[72] J. Carlson, J. Morales Jr., V. R. Pandharipande, and D. G. Ravenhall, Phys. Rev. C **68**, 025802 (2003).
[73] S. Gandolfi, A. Yu. Illarionov, F. Pederiva *et al.*, Phys. Rev. C **80**, 045802 (2009).
[74] A. Gezerlis and J. Carlson, Phys. Rev. C **81**, 025803 (2010).
[75] S. Gandolfi, J. Carlson, and S. Reddy, Phys. Rev. C **85**, 032801 (2012).
[76] S. Gandolfi, J. Carlson, S. Reddy, A. W. Steiner, and R. B. Wiringa, Eur. Phys. J. A **50**, 10 (2014).
[77] A. A. Usmani and F. C. Khanna, J. Phys. G: Nucl. Part. Phys. **35**, 025105 (2008).
[78] Manfredo P. Do Carmo, *Differential Geometry of Curves and Surfaces*, 1st ed. (Prentice-Hall, Englewood Cliffs, NJ, 1976).
[79] J. Sivardiére and J. Lajzerowicz, Phys. Rev. A **11**, 2090 (1975).
[80] Ph. Chomaz and F. Gulminelli, Phys. Lett. B **447**, 221 (1999).
[81] M. Dutra, O. Lourenço, and D. P. Menezes, arXiv:1510.02060.